Yonsei University - Shizuoka University Students Workshop 2011

Proceedings

December 5,2011

Yonsei University, Seoul, Korea

Yonsei University - Shizuoka University

Students Workshop 2011

Proceedings

December 5, 2011

Yonsei University, Seoul, Korea

Program

Yonsei University - Shizuoka University Students Workshop 2011

December 5, 2011 (Monday) at Yonsei University, Korea

Program

14:45-15:00 O-14

Cathodeluminescence Imaging of Metallic Nanostructures ·····37

Ryuji Noda, S. Fukada, Y. Nawa, A. Ono, W. Inami, D. G. Xiang,

S. Saito, and Y. Kawata (Shizuoka University)

15:00-15:15 **Closing Remark**

Proceedings

O-01

Autoconfocal transmission microscopy based on nonlinear detection

Chulmin Joo[1,*], Chun Zhan[2], Qing Li[2], and Siavash Yazdanfar[2]

[1]School of Mechanical Engineering, Yonsei University, 50 Yonsei-Ro, Seoul 120-749, Korea
[2]GE Global Research, 1 Research Circle, Niskayuna, NY 12309, USA
TEL&FAX: +82-2-2123-5822
[*]e-mail: cjoo@yonsei.ac.kr

Abstract

We describe a simple, self-aligned confocal transmission microscopy based on nonlinear optical detection with a silicon photodiode. Silicon detectors produce photocurrents in quadratic dependence on incident optical intensity under the pulsed illumination of light with wavelengths longer than 1.2 μm. We exploit this nonlinear absorption process to reject out-of-focus diffuse background and to perform depth-sectioning microscopic imaging. We demonstrate a comparable background rejection capability of our method to linear confocal detection, and present three-dimensional images of biological tissues.

1. Introduction

Laser-scanning confocal microscopy (LCSM) is capable of producing high-contrast, high-resolution images of biological specimens with depth-sectioning capability. The improved image contrast and depth resolvability in LCSM is enabled by a physical pinhole in the image plane, which allows in-focus portion of light to be measured while rejecting stray light from out-of-focus background. Among the various modes of operation in LCSM, the transmission mode, which measures the transmitted light through the specimen, has an advantage over the reflection (or epi-detection) mode, in that the transmitted light has higher intensity, alleviating a need for highly sensitive detectors (e.g. PMT). Yet, to acquire images, a dedicated mechanism is required to descan the beam or to move the pinhole synchronously with the illumination beam.

In order to address the issues, we developed a novel confocal transmission microscopy technique based on virtual confocal detection in a solid-state detector. The method, which we term autoconfocal microscopy (ACM), is based on the principle that pulsed light impinging on a semiconductor induces a photocurrent due to nonlinear absorption if the incident photon energy ($h\nu$) meets the condition $h\nu < E_g < nh\nu$, where E_g is the detector bandgap energy and n is the order of nonlinearity. Since this nonlinear response is highly dependent on temporal and spatial profile of incident pulses, the in-focus light generates markedly higher signal than the out-of-focus background. Moreover, the desired nonlinear absorption and the transformation of light into the electric current are combined into a single, readily available photodiode, which enables a simple and efficient implementation for confocal imaging. As a proof-of-concept, we present ACM operation based on nonlinear response of silicon photodiode (Si-PD) to ~1.55 μm fiber-based femtosecond laser.

2. Experimental Setup

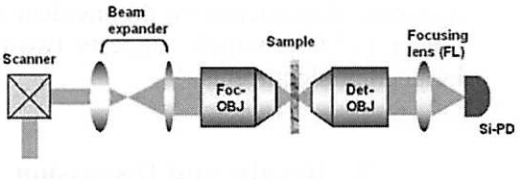

Fig. 1 Schematic of ACM. A beam from a ~1.55 μm femtosecond laser was employed as a light source. The light transmitted through the sample was focused onto and detected by the Si-PD. Foc-OBJ and Det-OBJ are microscope objectives for focusing and detection path.

Figure 1 depicts a schematic of ACM prototype. A ~1.55 μm light from the erbium-doped fiber laser (pulse width ~ 100

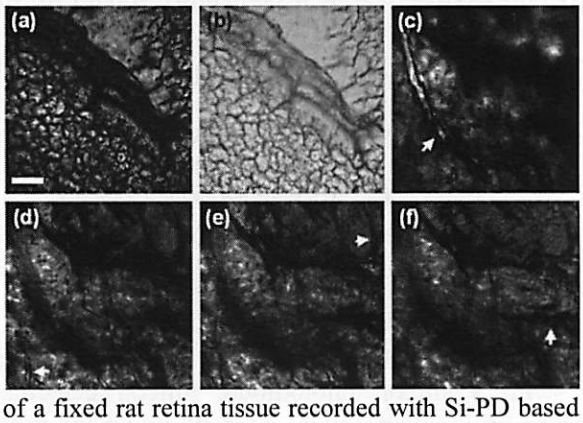

Fig. 2: (a)–(b) Images of a fixed rat retina tissue recorded with Si-PD based ACM and Ge-PD based linear detection, respectively. Note the improved image contrast provided by Si-PD based nonlinear detection. (c)–(f) Si-PD based ACM images of fixed rat choroid tissue at tissue surface and 20, 40, 60 μm below the tissue surface, respectively. Vascular structures and epithelium are clearly visible at each depth with high contrast. The scale bar represents 50 μm.

fsec and repetition rate ~ 50 MHz) is collimated, magnified, and focused onto the specimen via Foc-OBJ. The forward scattered light from the sample is then collected by the detection objective (Det-OBJ) and refocused onto Si-PD with a diameter of ~10 μm. The response of Si-PD under focused illumination of continuous (CW) and pulsed (PW) light at 1.55 μm was then examined. For the CW case, no signal was observed on the detector, since 1.55 μm light energy (~0.8 eV) is below the bandgap of Si (~1.12 eV). However, PW illumination resulted in a remarkable signal increase due to nonlinear absorption (data not shown). We examined the output signal as a function of the incident optical power for the PW case, and found that the signal exhibited a quadratic dependence on the incident optical power (~2.01), which suggests two-photon induced photocurrents.

3. Results and Discussion

Having observed nonlinear response of Si-PD to the employed femtosecond laser, the improved image contrast and rejection of out-of-focus background by ACM was assessed by imaging fixed rat retina. Figs. 2(a) and 2(b) show the images obtained with the Si-PD based nonlinear detection and germanium PD based linear detection (Ge-PD). While vascular and morphological structures were visible in both images, the out-of-focus background rejection capability in ACM resulted in a much higher contrast and more detailed morphological information. We also performed ACM imaging on a ~80 μm thick fixed rat choroid by scanning the sample along the optical axis to demonstrate three-dimensional imaging capability. The representative images at the tissue surface and in ~20 μm steps below the surface are shown in Figs. 4(c-f). The distribution of vascular structures and epithelium at different depths is clearly visible, while high image contrast is maintained.

4. Summary

A cheap and simple scheme for autoconfocal transmission microscopy was demonstrated. The self-aligned virtual pinhole was achieved by a single large-area silicon photodiode that generates photocurrents in a quadratic dependence on incident intensity of ~1.55 μm pulsed illumination. High-contrast, depth-resolved images of biological tissue samples were presented.

Reference

[1] C. Joo *et al.*, Opt. Lett. **35** 67-69 (2010)

O-02

Characteristic analysis of CFRP cutting with nanosecond pulsed laser

Keisuke Ushida[1*], Wataru Inami[2,3], Yoshinobu Shimamura[1], and Yoshimasa Kawata[1,3]

[1]Faculty of Engineering, Shizuoka University, [2]Shizuoka Univ. GRL, [3]JST-CREST
3-5-1 Johoku, Naka, Hamamatsu, Shizuoka 432-8561, Japan
TEL&FAX: +81-53-478-1076
E-mail: kawata@eng.shizuoka.ac.jp

Abstract

Carbon Fiber Reinforced Plastics (CFRP) have features of high specific strength, high rigidity, light weight, etc. The cutting techniques used for CFRP today are water-jet cutting and mechanical cutting operations such as sawing, milling, or grinding. However, they have problems of high tool-wear, wastewater disposal, etc. These disadvantages limit the applications of CFRP. We perform the cutting of CFRP with nanosecond pulsed laser and analyzed its characteristics. We investigated machining-depth dependences on the condition of focus position and the amount of overlapping area of focus spot on CFRP surface.

1. Introduction

Carbon Fiber Reinforced Plastics (CFRP) are composite material composed by carbon fiber and plastic resin. The features of the material include high specific strength, high rigidity, light weight, etc [1]. Therefore, CFRP have become an essential engineering material in many modern industrial applications[2].

The main cutting techniques used for CFRP today are water-jet cutting and mechanical cutting operations such as sawing, milling, or grinding. However, they have problems of high tool-wear, wastewater disposal, etc. Therefore, it is difficult to say that these processing methods are simply and easy way. The disadvantages limit the applications of CFRP.

Laser cutting is paid attentions because it has potentials solving the disadvantages of water-jet cutting and mechanical cutting operations [3]. We present laser processing characteristics with nanosecond laser pulse.

2. CFRP and laser source

In this study, 981 mm thick CFRP were used for laser processing. A ply was composed of unidirectional fiber and resin that harden fiber. It was laminated [0°/90°/90°/0°] orientation. We used a Q-switch Nd:YAG laser (wavelength = 532 nm, pulse width = 4 ns). Numerical aperture (N.A.) of the objective lens was 0.10.

3. Experimental Result and Discussion

We investigated the machining-depth dependence on scanning speeds with various focused positions. The focus position was varied in the region from -500 μm to 500 μm and scanning speeds were 0.2 μm/s, 0.4 μm/s, 0.8 μm/s, 1.6 μm/s. After laser irradiations, the machining depth and width were measured with scanning electron microscope (SEM). In these experiments, we scanned laser light only once.

Figure 1 shows SEM images of cross sections of laser processed CFRP. Figure 2 shows the results of the machining-depth dependence on each focus position with various scanning speeds. It was found that the machining depths were increased with the larger value of focused positions, and depths were limited at certain values. When the focus position was moved to the inside of the CFRP surface more, the machining depth decreased. The maxima of machining depths became smaller with higher scanning speed.

Fig. 1. Cross sections of processed CFRP.

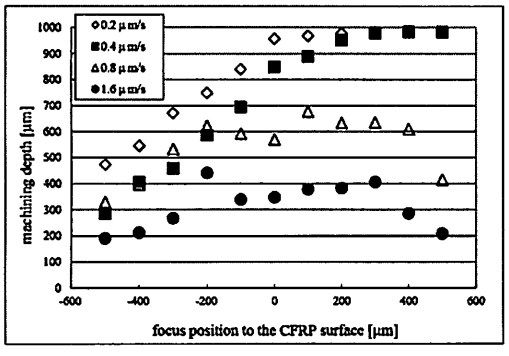

Fig .2. The machining depth for each scanning speed and focus position.

We also analyzed the machining-depth dependence on overlapping area of focused spot and number of laser scans. Figure 3 shows the overlapping condition of focus spot on CFRP surface. In each condition, laser beam was scanned with the number of 1, 5, 10, 20, 50, 100, 200 times. In these experiments, the focus position was fixed on the CFRP surface.

Figure 4 shows the dependence of the machining-depth on the condition of overlapping area of focus spot and number of laser scans. It was found that the machining depths became larger as the number of scans were increased. The machining depths also became larger as the size of overlapping areas were increased. We could also recognize that increasing rate of the machining depths to the increasing number of beam scan gradually became smaller. Focused spot was slightly defocused during the laser processing because the CFRP surface was mined by laser irradiations. Therefore, we may say that more efficient processing can be performed by adjusting the focus position into internal side on every scan.

	Overlapping condition	Spot interval [μm]
A		30
B		22.5
C		15
D		7.5

Fig .3. The condition of the size of overlap of focus spot on CFRP surface.

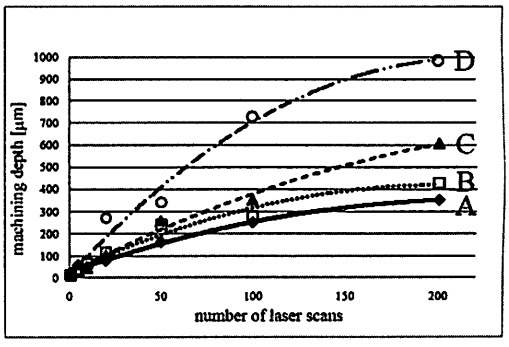

Fig .4. The dependence of the machining depth on the condition of overlapping area of focus spot and number of laser scans.

4. Conclusion

We investigated the machining-depth dependence on scanning speed with various focused positions. It was found that the optimum focus positions existed in each scanning speed in order to achieve large machining depths. It was found that there were threshold of the power density to process.

We also analyzed the machining-depth dependence on overlapping area of focused spot and number of laser scans. It was found that the machining depths also became larger as the size of overlapping areas were increased. We could also recognize that increasing rate of the machining depths to the increasing number of beam scans gradually became smaller.

As next research issues we should discuss the optimum processing conditions for decreasing process time. Heat effects induced by laser illumination on CFRP should be analyzed for fine laser processing.

References

[1] K. Tohgo, UCHIDA ROKAKUHO ,2004
[2] Dirk Herzog, Peter Jaeschke, Oliver Meier, Heinz Haferkamp, "Investigations on the thermal effect caused by laser cutting with respect to static strength of CFRP", International Journal of Machine Tools & Manufacture 48, 2008, pp. 1464–1473.
[3] K.C. Yung, S.M.Mei, T.M. Yue, "A study of the heat-affected zone in the UV YAG laser drilling of GFRP materials", Journal of Materials Processing Technology 122, 2002 p278-285

O-03

Dynamic Characteristics Prediction of the Perforated Cylindrical Shell in SMART Using Similarity Analysis

Young-In Choi, Seungho Lim, Young-Pil Park, No-Cheol Park, Kyoung-Su Park*

Department of Mechanical Engineering, Yonsei University
50 Yonsei-ro, Seodaemun-gu, Seoul, 120-749, Korea

TEL&FAX: +82-2123-3847
*e-mail: pks6348@yonsei.ac.kr

Abstract

This paper introduces dynamic characteristic identification of reactor internals using finite element method. The research also considers fluid-structure interaction between coolant water and reactor internals. The results are verified by comparing the results of the modal test. In addition, this paper introduces similarity analysis using NAVMI factor. From this factor, dynamic characteristics of submerged structures which have different scale factor can be predicted.

1. Introduction

Now Korean Atomic Energy Research Institute is developing the System-integrated Modular Advanced ReacTor (SMART). The SMART includes components like a core, steam generators, coolant pumps, and a pressurizer inside the one reactor vessel. Though the integrated structure improves the safety of the reactor, it can be excited by an earthquake and pump pulsations. It is important to identify dynamic characteristics of the reactor internals considering fluid-structure interaction. Thus, modal analysis with the modal test and the finite element method (FEM) is performed in order to identify the dynamic characteristics of the reactor internals.

The flow skirt, which is a perforated cylindrical shell, is located in the lower plenum of the reactor. In order to perform the modal test, a 1/12 size scale-similarity model is manufactured and finite element model is constructed based on this scale-similarity model. The dynamic characteristics of the similarity model are extracted by the modal test and FE model is verified by comparing the result between the modal test and the FE analysis. This study further carries out the similarity analysis for predicting the dynamic characteristics of the real reactor internals. The natural frequencies of the real reactor internals are calculated with the NAVMI factor and calibrating factors. Results of the similarity analysis are verified by comparing the results of the FE analysis.

2. Finite Element Model

The flow skirt has total 1668 holes which have a triangular pattern. It is reinforced by three circular ribs on the inside of the shell. Six lower flanges is located in the lower part of the flow skirt and they are fixed to hemispherical surface of the reactor vessel. A finite element model of a 1/12 scale-similarity model is built up and the finite element analysis is implemented by using commercial package, ANSYS. Figure 1 illustrates the finite element model of the flow skirt and surrounding fluids which is applied boundary conditions and the fluid-structure interaction.

3. Similarity Analysis

It is impossible to perform the modal test with large scale structures like the reactor. Thus, similarity analysis is used for predicting natural frequencies of the real reactor internals from the similarity model. Kwak [1] is expressed the influence of the added mass effect by the NAVMI (Non-dimensional Added Virtual Mass Incremental) factor. Natural frequencies of the submerged real reactor internals can be calculated from the natural frequencies of the scale-similarity model in the air by using the NAVMI factor.

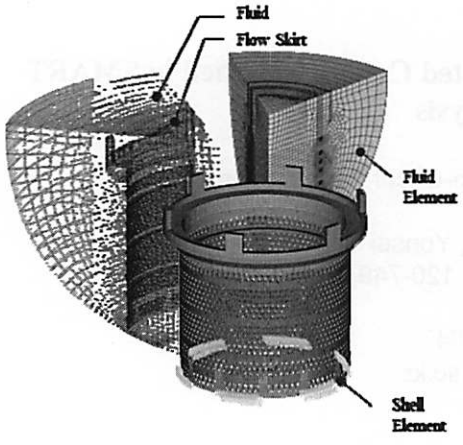

Fig.1 FEM Model of Flow Skirt

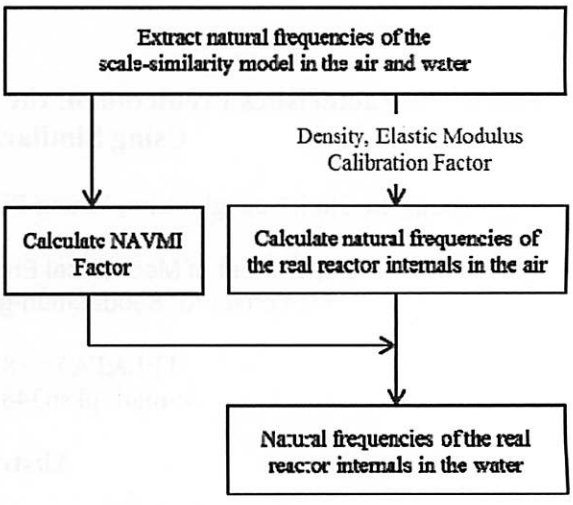

Fig.2 Process of Similarity Analysis

Table 1 Similarity analysis of flow skirt with NAVMI factor

Mode	1/12 Scale Similarity Model of Flow Skirt		NAVMI Factor	Real Size Model of Flow Skirt			
	Aluminum(air)	Aluminum(Water)		Steel(Air)	Steel(Water)		
	FEM	FEM		Calculation	Calculation	FEM	Error (%)
1	988.1	757	1.90	82.34	76.85	76.8	0.06
2	1097	789.3	2.52	91.41	78.63	78.8	-0.21
3	1974	1402	2.65	164.5	142.62	141.3	0.94

Fig.2 explains process of the similarity analysis. And next equation shows natural frequencies of the submerged real model.

$$f_{L,r} = \frac{f_{O,s}}{\kappa}\sqrt{\frac{\varepsilon}{\zeta_p(1+\zeta_m\Gamma_s)}} \quad (1)$$

3. Results and Discussion

Table 1 shows results of the similarity analysis. NAVMI factor is obtained by the natural frequencies of the scale-similarity model. From NAVMI factor, natural frequencies of the real size model of the flow skirt in the water are calculated. The calculated results are well matched with the results of the FE analysis.

4. Conclusion

In this research, dynamic characteristics of the flow skirt in the reactor are extracted by the finite element analysis. Furthermore, similarity analysis is carried out with the constructed finite element model. The NAVMI factor is used for calculating the natural frequencies of the real size model and these results compare with the results of the FE analysis. The results show validity of the similarity analysis.

Reference

(1) M. K. Kwak and K. C. Kim , 1991, "Axisymmetric Vibration of Circular Plates in Contact with Fluid," Journal of Sound and Vibration, 146(3), pp. 381-389

O-04

Two-Photon Excitation with Visible Femtosecond Laser for Observation of Wide-Gap Semiconductors

Kohei Takamatsu[1], Wataru Inami[2,3], Yoshimasa Kawata[1,3]

[1]Faculty of Engineering, Shizuoka University, [2]Shizuoka Univ. GRL, [3]JST-CREST
3-5-1 Johoku, Naka, Hamamatsu, Shizuoka 432-8561, Japan
TEL&FAX: +81-53-478-1076
E-mail: kawata@eng.shizuoka.ac.jp

Abstract

We have developed a technique of two-photon excitation in visible region, and applied to observe internal defects of ZnO crystal which emits photoluminescence in ultraviolet region (367nm). In order to observe a ZnO crystal, we introduced 521nm SHG femtosecond solid-state laser [1, 2] as a light source

1. Introduction

Semiconductor lasers in ultraviolet region have been developed by many researchers. Structure defects in the semiconductor crystal decrease the emission efficiency of the devices. In order to improve the device efficiency, it is required to reduce the structure defects in a crystal as much as possible in the stage of the crystal growth. Therefore, evaluation of a crystal becomes indispensable.

Two-photon excitation microscope is used for evaluation of a semiconductor crystal, and Ti:Sapphire laser is used as a excitation light source. Since wavelength region of typical Ti:Sapphire laser is 720-900 nm, wide-gap semiconductors cannot be excited with two-photon process. In order to observe a semiconductor crystal with a wider band gap, we introduced a SHG femtosecond solid-state laser as an excitation light source. We observed internal defects of ZnO crystals.

2. Two-photon excitation for evaluation of a crystal

The absorption of a typical semiconductor crystal in the wavelength region that is shorter than the wavelength λ_{bg}, which corresponds to band-gap energy of the material. Since the excitation wavelength should be shorter than the wavelength λ_{bg}, the excitation light is much absorbed in the material. Figure 1 shows comparison of excitation region between single- and two-photon excitation. In a single-photon excitation, the excitation light cannot penetrate into deep area of the material, because it absorbed during the propagation. This limits the usage of photoluminescence studies in three-dimensional observation.

Two-photon excitation will allow three-dimensional imaging of the crystals because the wavelength used in two-photon excitation is much longer than the wavelength λ_{bg}. Photoluminescence is excited only in the focal volume in two-photon excitation. Thus observation of the particular position inside a crystal is possible.

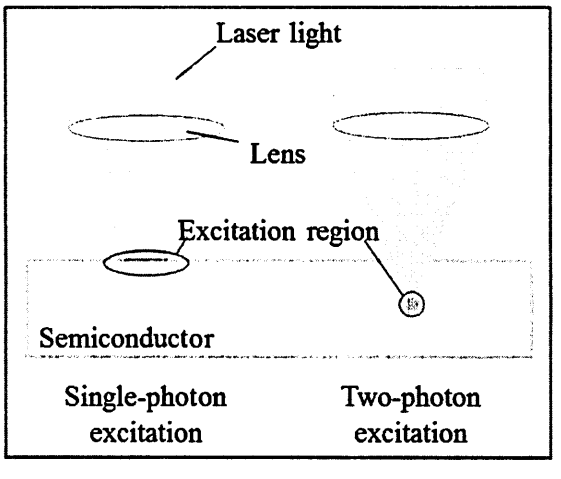

Figure 1. Comparison of excitation region

3. Observation of internal defects in ZnO crysta

Figure 2 shows the experimental setup of

two-photon excitation microscope. A SHG femtosecond solid-state laser (pulse width: 350fs, repetition: 2.85GHz) is used as a excitation light source, and scanned through the sample area using galvanometer mirrors.

In this research, we choose ZnO crystal as a sample for observation. Band gap of ZnO is 3.37 eV and wavelengths equivalent to this band gap energy is 368.9 nm.

Figure 3 shows results of observation of ZnO crystal to the depth of 10μm inside. We achieved three dimensional imaging of ZnO crystal, which emits luminescence in an ultraviolet region. The excitation region is limited near the focal point by two-photon processes, and we could also observe the outline of internal defects of a crystal.

Figure 4 shows comparison of cross-sectional profile of the marked position in Fig. 3. In a portion with a low quality crystal, a decrease in luminous efficiency occurs. It is thought of as an internal defect exists in the portion which is low intensity compared to the crystal surface.

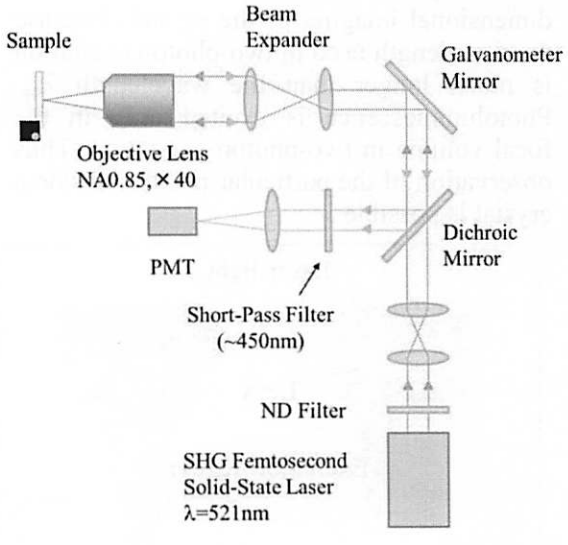

Figure 2. The experimental setup of two-photon excitation microscope

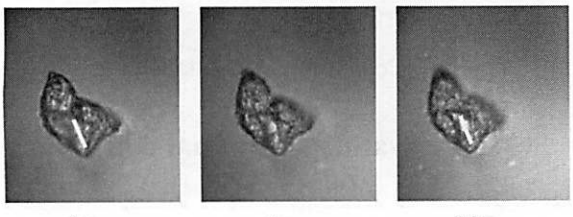

Figure 3. Result of the observation of ZnO

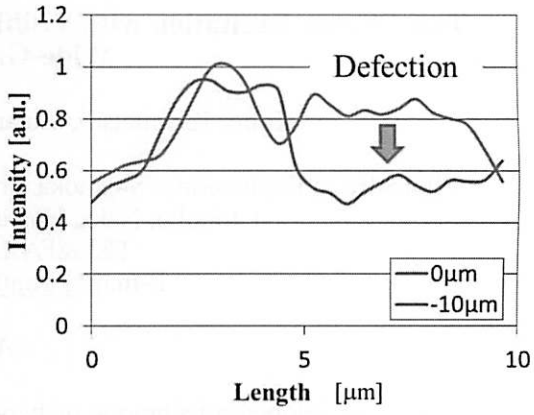

Figure 4. Comparison of cross-sectional profile

4. Conclusion

We introduced 521nm SHG femtosecond solid-state laser for excitation light source, and achieved three dimensional observation of ZnO crystal which emits light in ultraviolet region. We are try to extend our technique to observe other wide gap semiconductors, such as GaN and SiC. We also try ti get spectral information in order to identify the defects origins..

Reference

[1] S. Yamazoe et al., Opt. Lett., vol.35, No.5, pp. 748-750,2010.

[2] T. Kasamatsu et al., IWHM&D2009 paper 4F-1

O-05

Tracking Servo Method using Pre-patterns for Holographic Data Storage

Sung-Yong Lim, Hyunseok Yang*, Kyoung-Su Park, No-Cheol Park, and Young-Pil Park

Department of Mechanical Engineering, Yonsei Univ., 262 Seongsanno,
Seodaemun-Gu, Seoul, Korea
TEL&FAX: +82-2-2123-2824
*e-mail: hsyang@yonsei.ac.kr

Abstract

Page-oriented holographic data storage (HDS) is very sensitive to the disturbances which affect the position of the recording media. Therefore, more precise tracking servo is required for recording process and it is also essential for high density. Therefore, compensation method which is essential for the recording process is needed in HDS. In this paper, we suggest some pre-pattern for tracking servo in recording process. This method was motivated by the tracking servo method in Hard Disk Drive. For designing the pattern shape, HDS characteristics were considered. Secondly, the track error signals were analyzed. Lastly, intervals of the pre-patterns considering track tolerance were determined.

1. Introduction

Page-oriented Holographic Data Storage (HDS) is one of the most promising candidates for next-generation storages because of high density, high data transfer rate and short access time. Its large storage capacity is achieved by multiplexing scheme. The fast data transfer rate can be realized from its storage in page units. The one-page unit can include more than one million bits, so the data transfer rate can be faster than conventional Optical Disc Drive (ODD) [1]. However, the conventional off-axis HDS has some disadvantages of constructing tracking servo mechanism system. Therefore, various compensation methods considered for the HDS characteristics have been proposed. The previous researches for de-track compensation have limitation so that they are only available for retrieval process. Therefore, we suggest some pre-pattern for tracking servo in recording process. The method proposed in this paper was motivated by the tracking servo method in Hard Disk Drive (HDD). In decision parameters for proposed method, results from tolerance analysis by InPhase Cooperate were referred [2].

2. Pre-patterns Design

The eccentricity of the disc can be regarded as a major effect form the track error in the HDS. Others de-track sources like deviation and unbalance of disc cannot affect track error. Because, reading and recording processes are conducted with stop-go rotation mechanism.

Typical size of focused servo beam for tracking servo is in a few μm units. In simulations, focused beam size is $2.75\,\mu m$. However, the HDS disc has much bigger track pitch than focused servo beam spot because size of multiplexed hologram spot determined by polytopic filter is about $600\ \mu m$. To solve this problem, disc formatting and proposed patterns designing will be made as following procedure. First of all, data zone and servo patterns are placed in the disc, as shown in Fig. 1(a). Data tracks are included in the data zone. The data between servo patterns is recorded sequentially. The data overlap is available due to polytopic multiplexing [3], as shown in Fig. 1(b). A diagonal pattern is located between two straight patterns, as shown in Fig. 1(c). Patterns must be able to reflect the incident beam.

The Track Error Signal (TES) is generated by time difference among the three reflected beams from the pre-patterns. After disc is inserted over a tapered spindle, the disc is rotated with a constant speed until detecting one TES signals set. Although servo beam spot is significantly smaller than

the track pitch, linear TES can be generated by using propose method. In other words, this method has TES range which can cover the track pitch. The reflected servo beams from the patterns generate the TES, as shown in Fig. 2. When servo beam crosses the patterns, A, R, B, peaks times of the reflected beams are represented as T_A, T_R, T_B. TES is generated according to Eq. 1.

$$TES = (T_B - T_R) - (T_R - T_A) \quad (1)$$

Quantified TES due to the amount of eccentricity and rotation angle of disc is analyzed. First of all, parameters for analysis, where e is amount of de-track, δ is amount of eccentricity, r_o is distance from center of spindle to original beam spot, r_{eff} is distance from center of eccentricity disc to rotated beam spot, and r' is distance from center of eccentricity disc to rotated beam spot and θ is angle between r_{eff} and r_o.

Based on these parameters, de-track can be written as Eq. 2. Beam spot is on the disc which is r_o from center of spindle so that the proper data recording and retrieval process is possible. However, after the disc is rotated in θ for other data, distance between spindle and beam spot is changed as r', as shown in Fig. 3. Therefore, $|r' - r_o|$ can be defined as de-track.

$$e = |r' - r_o|$$
$$\left(r' = \sqrt{(r_{eff}\cos\theta + \delta)^2 + (r_{eff}\sin\theta)^2}, r_{eff} = r_0 - \delta \right) \quad (2)$$

Through the Eq. 2, it is certain that proper interval angle of servo track is $\theta = 30°$ with $\delta = 100um$ eccentricity and $25um$ de-track tolerance.

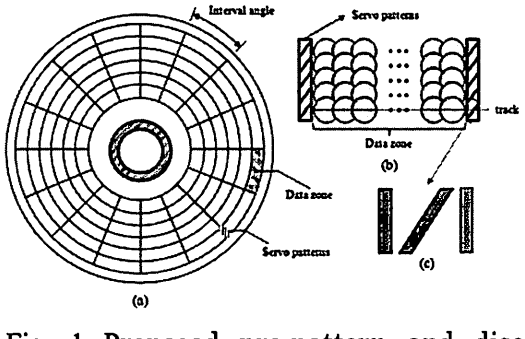

Fig. 1 Proposed pre-pattern and disc formatting

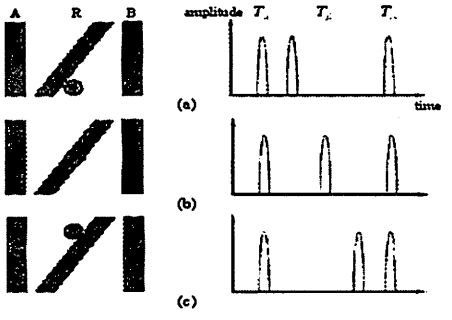

Fig. 2 TES due to direction of the track errors

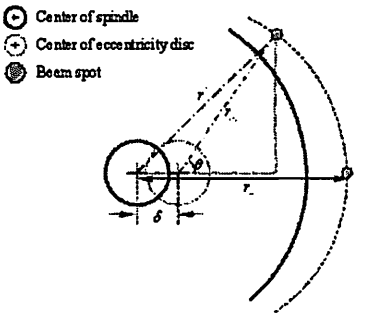

Fig. 3 Analysis of TES due to rotation of disc with eccentricity

3. Conclusion

In this paper, an adaptive de-track compensation method for conventional off-axis HDS was proposed. This method has an advantage that it can be applied to recording process differently from previous researches. Therefore, the high quality data pages can be reconstructed. Through the analysis and simulation, the proposed de-track compensation method was verified that it is enough to compensate de-track.

Reference

[1] Coufal H. J., Psaltis D., Sincerbox G. T., Holographic Data Storage, Heidelberg, Germany (Springer, 2000).

[2] Alan Hoskins, Brad Sisson, Friso Schlottau, Edeline Fotheringham, Kevin Curtis, "Tolerances of a Page-Based Holographic Data Storage System" Proc. of SPIE Vol. 6620.

[3] Ken Anderson and Kevin Curtis, "Polytopic multiplexing", OPTICS LETTERS / Vol. 29, No. 12 / 2004.

Surface Plasmon Resonance in Deep-UV Region

Masakazu Kikawada[1], Atsushi Ono[2,3], Wataru Inami[2,3],
Rentaro Akimoto[1], and Yoshimasa Kawata[1,3]*

[1]Faculty of Engineering, Shizuoka University, [2]Shizuoka Univ. GRL, [3]JST-CREST
3-5-1 Johoku, Naka, Hamamatsu, Shizuoka 432-8561, Japan
TEL&FAX: +81-53-478-1076
E-mail: kawata@eng.shizuoka.ac.jp

Abstract

We demonstrated the surface plasmon resonance(SPR) with deep-ultra-violet (Deep-UV) region. We found that aluminum is good material to excite SPR with Deep-UV light by calculations on reflectance using fresnel equation. We also demonstrated the excitation of SPR in Deep-UV region.

1. Introduction

There are many studies on surface plasmon resonance (SPR) and its applications have been developed in various fields[1]. SPR has many advantages, such as enhancement of electric field intensity, high sensitivity to refractive index change of sample near the metal surface. In many studies and applications of SPR, visible or near-infrared light source have used for excitation of SPR, because gold and silver have very good properties in that wavelength region. Few studies have been reported on the excitation of SPR using Deep-UV light.

We present to excite surface plasmon using Deep-UV light. Deep-UV light has higher photon energy than that of visible light, so SPR with Deep-UV light opens many applications such as enhancement fluorescence excitation, fluorescent observation of the non-labeled biological specimens. In this paper, we demonstrate the excitation of SPR with Deep-UV light.

2. Principle to excite SPR

We explain the principle of SPR. Surface plasmon can be excited with a evanescent light satisfying the dispersion relationship. When wavenumber vector of longitudinal wave and wavenumber vector of polarization parallel to incidence plane. Because distribution of the free electron in metal condenses parallel in surface.

Equation (1) shows the propagation constant of surface plasmon.

$$K_{sp} = \frac{\omega}{c}\sqrt{\frac{\varepsilon_m \varepsilon_s}{\varepsilon_m + \varepsilon_s}} \tag{1}$$

$$= \frac{\omega}{c}\sqrt{\frac{\mathrm{Re}[\varepsilon_m]\varepsilon_s}{\mathrm{Re}[\varepsilon_m]+\varepsilon_s}} + \frac{\omega}{c}\sqrt{\left(\frac{\mathrm{Re}[\varepsilon_m]\varepsilon_s}{\mathrm{Re}[\varepsilon_m]+\varepsilon_s}\right)^3}\frac{\mathrm{Im}[\varepsilon_m]}{2\mathrm{Re}[\varepsilon_m]}i$$

where ω is the angular frequency of surface plasmon, ε_s is the dielectric constant of the dielectric materials, and ε_m is the complex dielectric constant of the metal. Here, imaginary part of ε_m represents decay of surface plasmon. In order to excite SPR, we need a metal with negative real part and small imaginary dielectric constant. Figure 1 shows real part and imaginary part of the complex dielectric constant of gold (a) and aluminum (b).

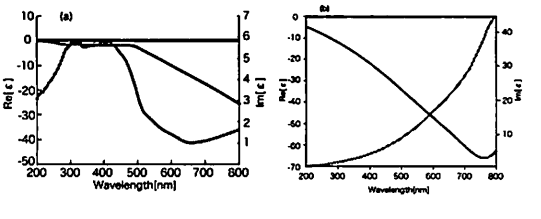

Fig.1. Complex dielectric constant of various metals (a) Gold (b)Aluminum

As shown in fig1(a), complex dielectric constant of gold has positive real part and large imaginary part in Deep-UV region. While complex dielectric constant of aluminum has a negative real part and small imaginary part and satisfies the conditions of SPR excitation in Deep-UV region.

3.Excitation SPR in Deep-UV region

We calculated reflectance for 3 layers model using Fresnel equations. Figure 2(a) shows reflectance dependence on the incident angle. The result of Al shows that the reflectance decreases approximately 0 at the angle of 45.4 degrees. At this angle, incident light couples with free electron in metal, incident photon excites SPR and the photon energy is transferred to the surface plasmon. On the other hands, the result at Au show the reflectance decreases gradually from the angle of 42 degrees in Deep-UV region. However this curve of Au does not have sharp dip and total reflection has not happened. So SPR can't be excited with Au in Deep-UV region.

Figure 3 shows experimental procedure and our experimental setup to measure reflectance. The method to create the thin Al film is vacuum evaporation and its controlled thickness is 21.4 nm. This thickness was determined by calculation at optimum thickness to excite SPR. The prism with thin Al film set on the rotation stage. We collected these data with changing incident angle to boundary between prism and metal. We measured the reflectance with the photodiode .

Figure 2(b) shows experimental results of reflectance with p-polarized light source. We found that the reflected intensity decreases at the angle of 55 degrees. This results that SPR can be excited on surface of Al. When we compare experimental result with calculation, we could also recognize that angle of dip was shifted in comparison with calculation result shown in Fig.2. The shift is caused by produced oxidization of Al surface produced. We need to evaluate thickness of oxidization of Al surface.

4. Conclusion

We demonstrated that Al is a good material to excite surface plasmon with DUV light. Experimental results show the excitation of SPR. As a result, reflected intensity decreases at the angle of 55 degrees. We demonstrated SPR excitation in Deep-UV region. We think that Deep-UV-SPR has unique application for various fields.

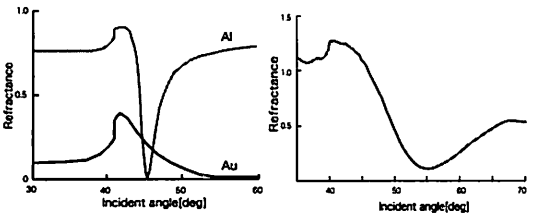

Fig.2. Experimental result: (a) Calculations for 3layers with consideration of Al and Au. Refractive index of Al, Au, and excitation wavelength are n_{Al}=0.16+2.62i, n_{Au}=1.38+1.80i, and 266 nm respectively. (b) Experimental result of thickness that 21.4 nm Al film at 266 nm wavelength.

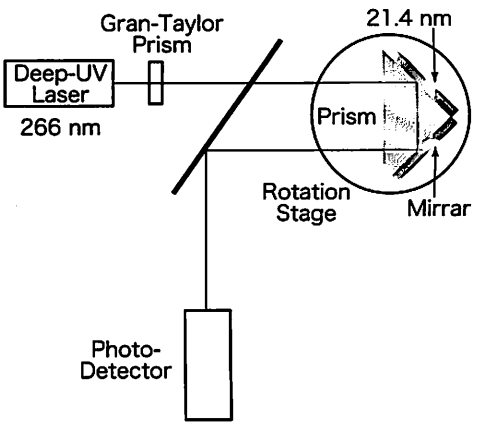

Fig.3. Experimental setup. Deep-UV Laser wavelength 266 nm, Al film 21.4 nm.

Reference

[1] Keiko Tawa, Hironobu Hori, Kenji Kintaka, Kazuyuki Kiyosue, Yoshiro Tatsu, and Junji Nishii *OPTICS EXPRESS* 9781 (2008) Vol.16., No.13.

O-07

Tribological Properties of ZnO Nanowires

Hae Jin Kim, Kyeong Hee Kang, and Dae-Eun Kim*

Department of Mechanical Engineering, Yonsei University,
50 Yonsei-ro, Seodaemun-gu, Seoul 120-749, Korea
TEL&FAX: +82-2-2123-7424
*e-mail: kimde@yonsei.ac.kr

Abstract

ZnO nanowires have received much interest over the past years due to their unique structure and piezoelectric behavior. In many applications of ZnO nanowires, the tribological properties of the nanowires need to be clearly understood. In this presentation the tribological characteristics of vertically grown ZnO nanowires studied under various conditions are reviewed. Particularly, the frictional behavior and wear characteristics of the ZnO nanowires are discussed. The results presented are expected to aid in improving the durability of ZnO nanowires.

1. Introduction

Coatings have been widely exploited to attain superior friction and wear properties of various components and continued efforts are being made to gain better understanding of their tribological behaviors.

Over the past years, much work has been done to develop nanowires of different materials for numerous engineering applications. Nanowires are interesting materials owing to their unique structure and size [1-3].

In previous works, the contact damage characteristics of ZnO nanowires grown vertically on a silicon substrate were investigated [4]. The frictional behavior under different scales of load was investigated by performing contact sliding experiments [5].

2. Experiment

The morphology of ZnO nanowires depends on the processing condition. ZnO nanowires in this study were made by two different methods, an aqueous solution method [6] and metal organic chemical vapor deposition (MOCVD) method. In Fig. 1, the SEM image of a typical ZnO nanowire specimen synthesized by the aqueous solution method is shown.

Contact sliding tests were performed under different loads. The wear track was observed to characterize the contact damage of ZnO nanowires for each load.

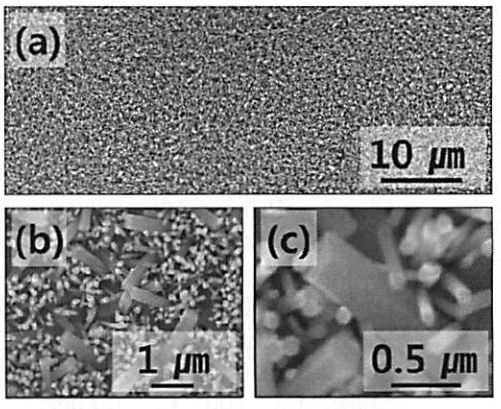

Fig. 1 SEM images of ZnO nanowires (a) evenly coated on Si wafer and (b), (c) at higher magnification

3. Results and Discussion

The contact sliding tests were conducted using the ZnO nanowire specimens under various loads while obtaining the frictional force. In micro-scale, the friction coefficient was about 0.35 for different applied loads throughout the entire sliding cycles. Under the low normal load, the wear rate of ZnO nanowires could be quantified by calculating the volume difference of the contacting parts.

4. Conclusion

In this research the contact damage characteristics and frictional behavior of ZnO nanowires were investigated. Based on

the results, tribological characteristics and failure mechanism of ZnO nanowires were assessed.

Acknowledgement

This work was supported by the National Research Foundation of Korea (NRF) grant funded by the Korea government (MEST).
(No. 2011-0000409)

Reference

[1] X. Sheng, Q. Yong, X. Chen, W. Yaguang, Y. Rusen and W. Zhong Lin, "Self-powered nanowire devices", Nat. Nanotechnol., **5** (2010) 366-373.

[2] L. Li-Yu, S. Ji-Min, J. Min-Chang, K. Kyung-Jin, K. Dae-Eun, M. Jae-Min, "Wear rate of vertically grown ZnO nanowires sliding against steel micro-sphere", Mater. Sci. Eng. A-Struct. Mater. Prop. Microstruct. Process., **460-461** (2007) 370-376.

[3] H. Woong-Ki, S. Jung Inn, H. Dae-Kue, K. Soon-Shin, J. Gunho, S. Sunghoon, K. Seong-Min, K. Hang-Ju, P. Seong-Ju, W. Mark E., and L. Takhee, "Tunable Electronic Transport Characteristics of Surface Architecture-Controlled ZnO Nanowire Field Effect Transistors", Nano Lett., **8** (2008) 950-956.

[4] K. Kyeong Hee, K. Hae Jin, and K. Dae-Eun, "Characteristics of Progressive Damage of ZnO Nanowires during Contact Sliding under Relatively Low Loads", J. of Nanomat., (2011).

[5] L. Li-Yu, S. Ji-Min, J. Min-Chang, K. Kyung-Jin, K. Dae-Eun, and M. Jae-Min, "Wear rate of vertically grown ZnO nanowires sliding against steel micro-sphere", Mat. Sci. & Eng. A, **460-461** (2007), 370-376.

[6] Q. Ahsanulhaq, A. Umar, Y. B. Hahn, "Growth of aligned ZnO nanorods and nanopencils on ZnO/Si in aqueous solution: growth mechanism and structural and optical properties", Nanotechnology, **18** (2007) 115603.

Cell processing with electron beam

Ken Watanabe[1*], Wataru Inami[2,3], and Yoshimasa Kawata[1,3]

[1]Department of Mechanical Engineering, Shizuoka University, Japan
[2]Division of Global Reserch Leaders, Shizuoka University, Japan, [3]JST, CREST
3-5-1 Johoku, Hamamatsu, Shizuoka, Japan
TEL&FAX: +81-53-478-1076
[*]e-mail: watanabe.ken@optsci.eng.shizuoka.ac.jp

Abstract

We present characteristic evaluation of cell processing using an electron beam, in order to realize nanometric fabrication. In this experiment, irradiation areas were observed with a phase-contrast microscope and an atomic force microscope.

1. Introduction

Nanotechnology has been studied for medicine and biology applications. The technology of processing cells is studied in research of cancer treatment and genetic engineering. Figure1 shows an example of cells cutting by laser ablation[1]. Laser processing has the resolution of hundreds of nm-order by focused light.

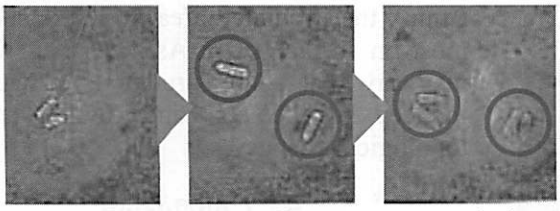

Fig.1. The yeast cell was separated by femtosecond laser. It can be confirmed that the laser processing was achieved without any damage on the cells.

In this research, we present to use an electron beam instead of laser for cell processing. It is expected that the electron beam can be used for fabricating in a nanometric region since the electron beam can be focused to a few tens of nanometer. In this experiment, we irradiate an electron beam on fixed and dried cells, and investigate damages on the cell.

2. The experimental setup which irradiates with an electron beam

Figure2 shows a schematic diagram of scanning of electron beam. The electron beam was irradiated as circle shape by scanning operation.

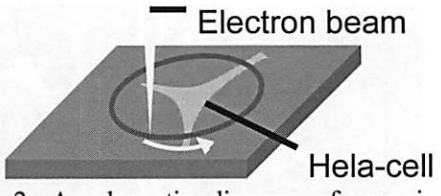

Fig.2. A schematic diagram of scanning of electron beam.

For irradiating an electron beam on a cell, a scanning electron microscope (SEM) was used. The cells used in the experiment are Hela cells which were cultured on a slide glass, and they were fixed and dried in order to process in a vacuum.

Figure3 shows the schematic view of the experimental setup for electron beam irradiation. A scanning coil is controlled by external current from a function generator to scan the electron beam with an arbitrary shape.

Accelerating voltage of the electron beam is changed as 20kV, 10kV, 5kV, 2.5kV. The irradiation area is the same on all conditions (magnification: × 800). Amount of electrons are same amount in all conditions.

3. Observation after irradiating

After irradiating electron beam on a cell, it was observed with the optical phase microscope and the atomic force microscope.Figure4 and Figure5 show observation results when it irradiates electron beam of 20kV of accelerating voltage. In a phase microscope, irradiated area is recognized clearly as the line shape on the cell surface.

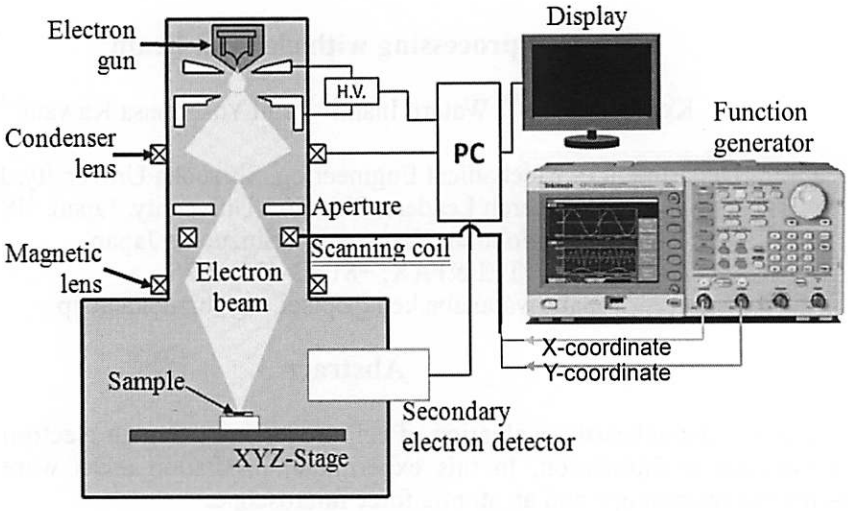

Fig. 3. An experimental setup when irradiating with electron beam

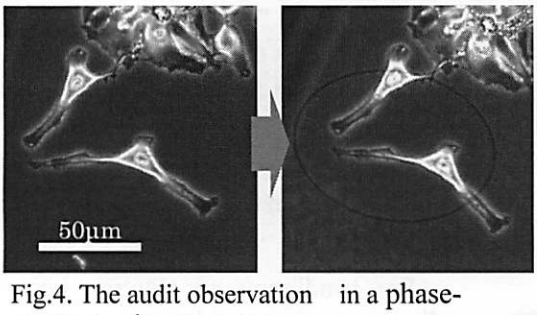

Fig.4. The audit observation in a phase-contrast microscope

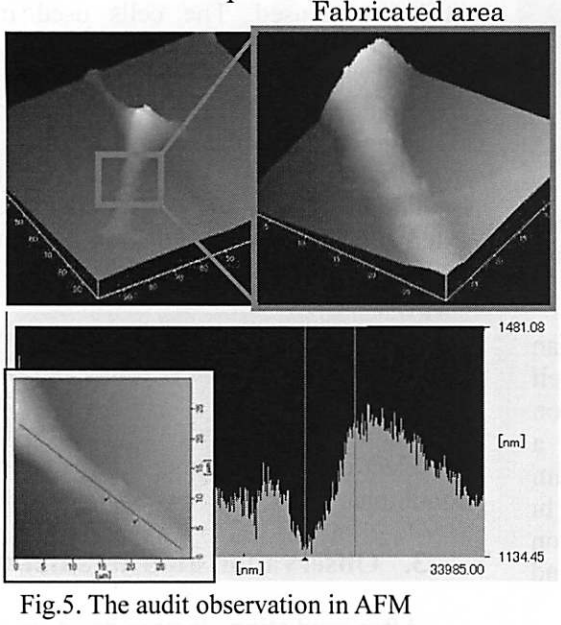

Fig.5. The audit observation in AFM

In the observation result by AFM, a depth of dent about 170-nm was produced at the irradiated area. The depth of dent was 130-nm when the accelerating voltage was 10kV. With the irradiation of 5kV and 2.5kV, it was difficult to recognize the dents on the cells.

4. Discussion

We could observed clear change in contrast through a phase contrast microscope. There were surely change on surface shapes of 20kV and 10kV, but it is very small change.

Compared with laser, the permeability of electron beam is low and energy of it is high. I think the irradiated area of cell is shocked most on surface of it. As a result of it, We may say that some structural change was induced in the cell and there were no topological changes.

5. Conclusion

As a next research issue, we need to investigate change of a cell in three dimensions using a confocal microscope. We would like to optimize the conditions of the amount of electrons, or focused spot size. Finally, we would like to conduct the experiment using the EXA-microscope[2]. It is possible to processing cells in atmosphere, and we can experiment and observe with living cells.

Reference

[1] Japan Science and Technology Corporation, www.jst.go.jp/pr/report/report226/, (11/15/2011).

[2] Y.Nawa, W.Inami, A.Ono, A.Miyakawa, Y.Kawata and S.Terakawa, Proceedings of 11th International Conference on Near-Field Optics, (2010).

Precision machining of GC mold

Wonkyun Lee, Kyung-In Jang, and Byung-Kwon Min*

School of Mechanical Engineering, Yonsei University,
50 Yonsei-Ro, Seodaemun-Gu, Seoul 120-749, Korea
TEL&FAX: +82-2-2123-5813 / +82-2-364-6769
*e-mail: bkmin@yonsei.ac.kr

Abstract

This paper introduces a novel machining process of glassy carbon (GC) surface utilizing the electrochemical oxidation. Hard and brittle materials can be machined by the synergy effect of mechanical machining and electrochemical reaction. A series of experiments were performed to verify the advantages of the proposed process.

1. Introduction

Glassy carbon (vitreous carbon, GC) is preferred as a mold material to be used in glass molding press (GMP) because of its high hardness and thermal stability. Furthermore, the cohesion between GC and glass is relatively weak. [1] However, it is hard to machine the complex shapes on GC surfaces because the GC is a brittle material with a high hardness (Shore hardness > 100). Alternative machining processes such as sawing, laser ablation and focused ion beam (FIB) have been proposed for precision machining of GC. [2-4] Wafer sawing is a simplest process, but, it is limited to machine simple features such as straight channel. [2] Direct laser ablation using a pulsed UV laser is suitable for rapid prototyping of complex shapes. However, it has limitation in form accuracy because of the beam shape. [3] FIB milling of GC can achieve nanometer scale accuracy, but, machining speed is extremely slow and the machining area is micrometer range. [4]

To overcome the above limitations, a novel machining process using the synergism of electrochemical oxidation and mechanical machining is proposed. A softened surface is generated on GC surface as a result of electrochemical oxidation, and mechanically removed.

In this study, experimental investigations of the effect of electrochemical oxidation on machining were performed. The machining results of the proposed method and conventional milling were compared to demonstrate the feasibility of the proposed process.

2. Experimental

Fig. 1 illustrates the process mechanism of proposed process: (a) Electrochemical equilibrium on surface are broken by applying overvoltage between GC workpiece (Tokai Carbon) and Pt counter electrode (ALS). An oxide layer is generated on GC surface. (b) The oxide layer is easily removed by a tool made of ZrO_2 because its

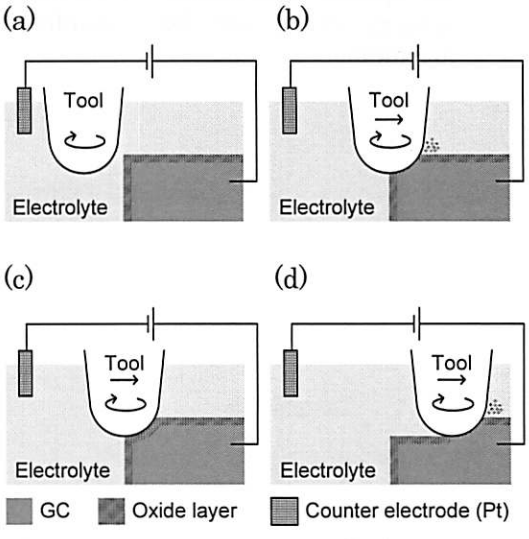

Fig. 1 Electrochemical oxidation assisted micromachining processes: (a) formation of oxide layer before machining, (b) removal of oxide layer and GC, (c) regeneration of oxide layer, and, (d) micromachining of GC by the repetition of the (b) and (c)

hardness is lower than that of GC. [4] If the stress applied on GC exceeds the fracture stress, cracks are generated on the machined surface. Therefore, the stress applied on GC should be controlled to avoid the crack propagation. (c) New oxide layer is regenerated on the newly exposed fresh GC surface. (d) The generation–removal–regeneration of oxide layer is repeated during the whole material removal process. Note that the normal force monitored and controlled during machining.

To investigate the effect of electrochemical oxidation on material loss, the various overvoltages (0.2V to 1.2V with 0.2V step) were applied in the middle of the line machining. Machining conditions such as normal force, tool rotation frequency and horizontal feed rate were maintained at constant values.

3. Results and Discussion

Cross sectional area of line was increased more than 30% in the region where the overvoltage of 1.2V was applied. The material loss is enlarged by the synergy effect from mechanical machining and electrochemical oxidation. Also we could verify that the material loss is proportional to the applied overvoltage. It means that the synergy effect can be controlled during machining.

4. Conclusions

In this paper, an electrochemical oxidation assisted micromachining process was proposed and experimentally verified.

Base on the experimental results the proposed method is considered as a promising fabrication method for 3D machining of GC molds and devices.

References

[1] M. Takahashi, K. Sugimoto and R. Maeda, Japanese Journal of Applied Physics **44** (2005) 5600-5605.

[2] S.W. Youn, M. Takahashi, H. Goto and R. Maeda, Journal of Materials Processing Technology **187-188** (2007) 326-330.

[3] M. Kuhnke, T. Lippert, E. Ortelli, G.G. Scherer and A. Wokaun, Thin Solid Films **453-454** (2004) 36-41.

[4] S.W. Youn, M. Takahashi, H. Goto and R. Maeda, Journal of Micromechanics and Microengineering **16** (2006) 2576-2584.

[5] K.-I. Jang, J. Seok, B.-K. Min and S.J. Lee, International Journal of Machine Tools and Manufacture **50** (2010) 869-881.

O-10

Optically controllable electrophoresis with a photoconductive substrate

Taiki Nagashima[A], Takafumi Iwahashi[A], Wataru Inami[B, C], Atsuo Miyakawa[A, C], and Yoshimasa Kawata[A, C]

[A] Faculty of Engineering, Shizuoka University, Japan

[B] Division of Global Research Leaders, Shizuoka University, Japan

[C] Japan Science and Technology Agency, CREST, Japan

e-mail: kawata@eng.shizuoka.ac.jp

Abstract

We develop optically controllable electrophoresis with a photoconductive substrate. We demonstrate simultaneous manipulation of microparticles without any flow channels.

1. Introduction

Micro Total Analysis Systems (μTAS) and Lab-on-a-chip have been developed in a medical and biological applications, and they have been intensively studied. The systems are expected to have more quick procedures and higher functionality.

Objective of this study is to control microparticles in fluid with laser irradiation. By combining property of photoconductive substrate and electrophoresis, we can achieve microparticles operation without flow channel. We believe that this technique contribute to development of the high functionality analysis devices.

2. Experimental setup of optical microparticles control

2.1 Photoconductive substrate

Photoconductive substrate is a kind of semiconductor, and its conductance is increased by a laser irradiation. When the photoconductive substrate is applied a voltage, potential gradient which related to resistance of substrate arise. On the photoconductive substrate, potential gradient is reduced in the region that the laser was irradiated because conductance of irradiated area is increased. Figure 1 shows schematic diagram of principle of photoconductive substrate. $Bi_{12}SiO_{20}$ (BSO) is used as photoconductive substrate[1, 2].

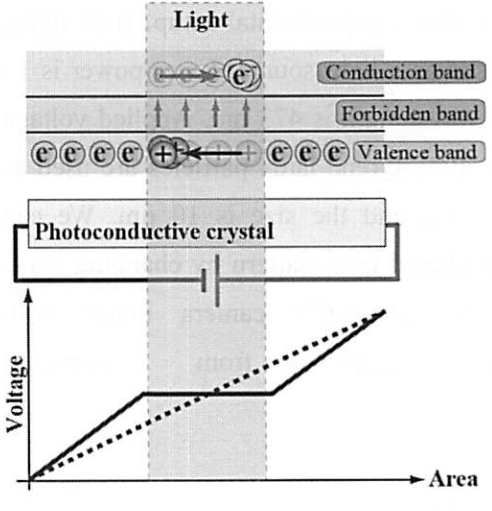

Fig. 1 Schematic diagram of principle of photoconductive substrate. Dashed line indicates potential gradient without laser irradiation. Solid line indicates potential gradient with laser irradiation.

2.2 Electrophoresis

Figure 2 shows principle of electrophoresis. Electrophoresis is the motion of dispersed particles relative to a fluid under the influence of

a spatially uniform electric field. The dispersed particles have electric surface charges, on which an external electric field exerts an electrostatic Coulomb force. Velocity and direction of particles depend on potential gradient. As a result of it, if we control the potential gradient, we can control microparticles movements.

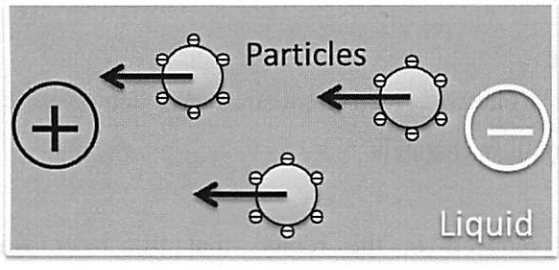

Fig. 2 Principle of electrophoresis. Particles with negative electrical charges move to positive electrode.

2.3 Experimental condition

Figure 3 shows experimental setup. Blue diode laser is used as a light source. Laser power is 15 mW, and wavelength is 473 nm. Applied voltage is 3.5 kV. Polystyrene latex particles are used as microparticles, and the size is 10 μm. We can control irradiated laser pattern by changing mask pattern and get CCD camera image with scattering light from particles.

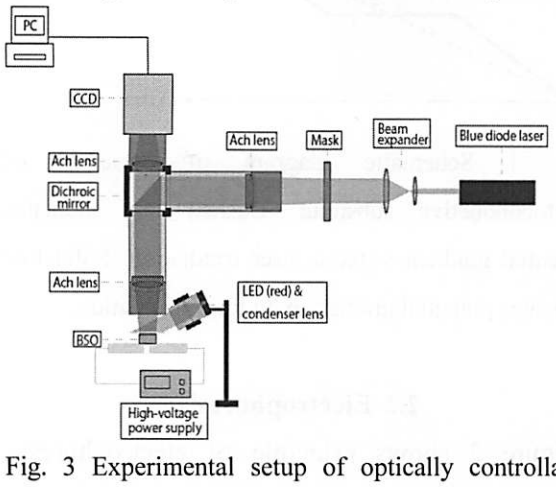

Fig. 3 Experimental setup of optically controllable electrophoresis with a photoconductive substrate.

3. Results of electrophoresis on the BSO with laser irradiation

Figure 4 shows CCD camera image of electrophoresis on the BSO substrate. The particles move from negative electrode to positive electrode along potential gradient without laser irradiation. On the other hand, when the laser is irradiated, potential gradient of the region near the irradiated area becomes steep. The particles collect around irradiated area.

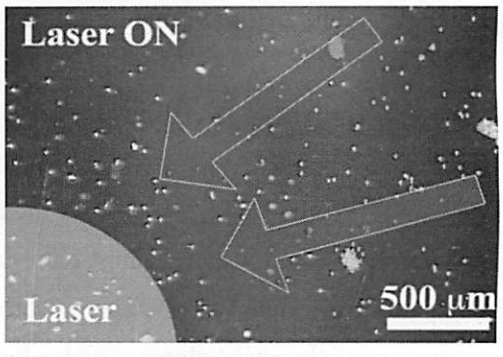

Fig. 4 CCD camera image of electrophoresis on BSO substrate. Circular laser pattern is irradiated on the BSO substrate.

4. Conclusion

We developed optically controllable electrophoresis with a photoconductive substrate. We can control microparticles by laser irradiation without processing flow channel.

References

[1] R. E. Aldrich, S. L. Hou, and M. L. Harvill, "Electrical and Optical properties of $Bi_{12}SiO_{20}$" *J. Appl. Phys.*, **42**, (1971) 493.

[2] M. Peltier and F. Micheron, " Volume hologram recording and charge transfer process in $Bi_{12}SiO_{20}$ and $Bi_{12}GeO_{20}$, " *J. Appl. Phys.*, **48**, (1977) 3683.

O-11

Fabrication of Antireflection surface via Nanosphere Lithography

Haesung Park, Kyoungsik Kim*
School of Mechanical Engineering, Yonsei University,
50 Yonsei-ro, Seodaemun-gu, Seoul 120-749, Korea
TEL&FAX: +82-2-2123-5815
*e-mail: kks@yonsei.ac.kr

Abstract

In this paper, we investigate optical absorption characteristic of the subwavelength antireflection surfaces which are fabricated by single-step deep reactive ion etching with nanosphere lithography. By integrating conventional quarter-wavelength antireflection coating and Si nanoconical-frustum, we successfully extend the antireflection bandwidth incldluing near-UV region without fabricating sub-300nm nanostructure.

1. Introduction

After first demonstration of solar cell, many researchers have been strived to improve photovoltaic efficiency and an economical rationality. Due to the innate high refractive index value of silicon (Si) material, Si based solar cell suffer from a low absorption of the solar energy. Therefore the cost reduction and absorption enhancement become a major interest in photovoltaic technology. The surface texturing (such as inverted pyramid etc.) developed for an enhanced light trapping in bulk Si over broad spectral range and wide incident angle. This could be a better solution than the quarter-wavelength antireflection coating which can only improve the absorption of a specific wavelength range and limited angle of incident solar energy. However, due to the thickness limitation, this strategy cannot directly compatible with thin film Si solar cell, which is about two order of magnitude thinner and cheaper than bulk Si solar cell. Recently, new strategy of enhanced light absorption based on nanostructure, such as Si nanocone (SiNC) [1] and Si nanowire (SiNW) [2] is proposed. These nanostructures can provide a gradually increased nanoscale refractive index structure and minimize reflection arising from refractive index difference at the Si and air interface.[3] Therefore, it is necessary to investigate the correlation between absorption characteristic and geometry of Si nanostructure.

In this paper, we have fabricated AR nanoislands on Si nanoconical-frustum array by using nanosphere lithography and single-step deep reactive ion etching. And we have investigated total (spectral and diffused) absorption and reflection property of nanostructures on crystalline Si substrate based on UV/VIS spectrometer with integrating sphere.

2. Sample preparation

Our approach to highly ordered Si nanostructure using self-assembled nanosphere lithography is composed of two steps. The first step is deposition of polystyrene (PS) nanosphere mask. And the second step is inductively coupled plasma (ICP) etching. Before the deposition, p-type (1 0 0) crystalline silicon substrates were cut in to pieces of 20mm x 20mm^2. Every pieces were cleaned with standard RCA I process (kept in a solution of NH_4OH (25%), H_2O_2(30%), and water at 80℃ for 15min) to make hydrophilic Si surface.

The deposition of PS sphere (dia. = 500nm, 360nm), begins from introducing of a nanosphere mixture solution on the surface of deionized water (18 MΩ·cm) in a large petri dish (dia. = 20cm). The mixture solution consists of ethanol and nanosphere water suspension (10% w/v) with proper ratio. As you can see the inset of Fig. 1(a), only when we make the suitable mixture concentration, we can see the iridescent color from a monolayer of highly ordered 2D close packed PS nanosphere on the water.

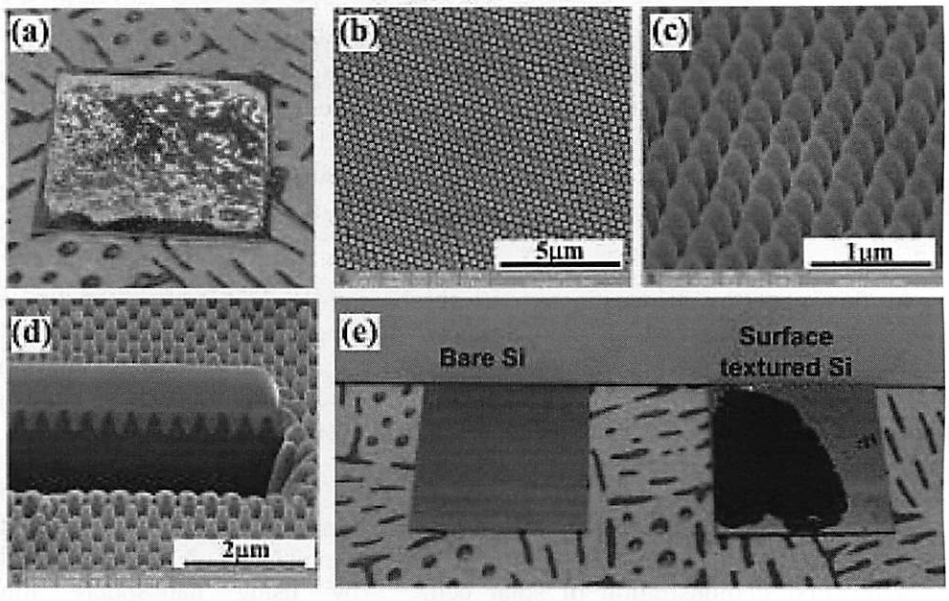

Fig. 1 (a) An optical photograph and (b) a SEM image (normal view) of 2D PS nanospheres monolayer mask pattern transferred on Si substrate (20 x 20 mm). (c) SEM image of PS sphere islands on top of Si NCF arrays while NCF arrays are fabricated via ICP etching. (d) Captured side wall profile image using a dual-beam FIB system. (e) A photograph of bare silicon and surface textured silicon.

Subsequently, the deionized water is drained and evaporated. Finally, the monolayer of nanosphere was slowly transferred onto the silicon substrate located beneath the petri dish.

3. Experimental Results

In order to characterize the reflectance of our samples, we performed absolute hemispherical measurement using UV-VIS-NIR pectrophotometer (UV3600, Shimadzu Scientific Instruments) with a 60mm-diameter integrating sphere (MPC-3100) by scanning a monochromator coupled to a halogen lamp. The average reflectance of our structure in the NUV spectral range (300~400nm) is significantly reduced to 3.8%, while that of sharp-tipped nanocone structures is as much as 9.2%.

The further details of our experimental results are discussed at the conference.

4. Conclusion

The antireflection property of our design is significantly enhanced compared to that of sharp-tipped nanocone structures, so that the average reflectance in the NUV spectral range (300~400nm) decreased from 9.2% to 3.8%.

To our best knowledge, this is the first method to extend antireflection spectrum including the NUV region without any complicated process to fabricate feature size below 300nm.[4]

Reference

[1] J. Zhu, Z. Yu, G. F. Burkhard, C. Hsu, S. T. Connor, Y. Xu, Q. Wang, M. McGehee, S. Fan, and Y. Cui, Nano Lett., **9** (2009) 279-282.

[2] K. Peng, Y. Xu, Y. Wu, Y. Yan, S, Lee, and J, Zhu, Small, **1**(2005), 1062-1067.

[3] S. Chuang, H. Chen, J. Shieh, C. Lin, C. Cheng, H. Liu, and C. Yu, Nanoscale, **2** (2010), 799-805.

[4] **H. Park**, D. shin, G. Kang, S. Baek, **K. Kim***, and W J. Padilla, *"Broadband optical antireflection enhancement by integrating antireflective nano-islands with silicon nanoconical-frustum arrays"*, Advanced Materials, **Accepted**, (2011).

Analysis of light and electron scattering in a thin film for EXA optical microscope

Masahiro Fukuta[1], Wataru Inami[2,3], Atsushi Ono[2,3], and Yoshimasa Kawata[1,3]

[1]Faculty of Mechanical Engineering, Shizuoka University, Japan
[2]Division of Global Research Leaders, Shizuoka University, Japan
[3]Japan Science and Technology Agency, CREST, Japan
E-mail: kawata@eng.shizuoka.ac.jp

Abstract

We analyzed the light and electron beam scattering in a nanometric thin film. We have developed a new analysis method that combines Monte Carlo simulation and FDTD (Finite Difference Time Domain) method. The Monte Carlo simulation is used to analyze electron beam scattering, and the FDTD method is to analyze light scattering. We coat a gold thin film on the fluorescent film to cut the electron beam transmission. The thickness of the gold thin film is 20 nm. As a result, the electron beam transmission was 0 %, and the full width at half maximum was 47.1 nm at the plane which is 10 nm away from the surface of the gold thin film.

1. Introduction

The electron beam excitation assisted optical microscope (EXA optical microscope) is a new microscope which can observe specimens in the living state with high resolution. The EXA optical microscope employs a nanometric light source which is generated in a fluorescent film by electron beam irradiation.[1]

Disadvantage of the EXA optical microscope is the damage for the specimen due to the electron beam transmission of fluorescent film. The transmission is high nearly 100 % when the incident energy is over 3 keV. Our research objective is to eliminate the damage on specimens by the electron beam. To achieve this objective, we coat a gold thin film on a fluorescent film.

We analyzed the electron beam and light scattering of nanometric light source in the fluorescent film coated a gold thin film. We use a new analysis method that is combination of Monte Carlo method and FDTD method. The electron beam scattering in the fluorescent film was analyzed by Monte Carlo simulation. The fluorescence excited by electron beam was analyzed FDTD method.

2. Analytical method

Figure 1 shows schematic of electron beam scattering. The electron scatters at P_0 to P_3 in this figure. We call P_0 to P_3 scattering position. When the electrons are irradiated the fluorescent film, they propagate straightly in the distance ΔS_n of mean free path, and change pathway due to scattering at atoms. We analyzed the electron beam scattering by calculating the distance ΔS_n and scattering angle θ_n, ϕ_n for each electron.

The electron losses the energy as it passes through the mean free path. The dipoles were excited by the energy loss as the electron passes through the mean free path.

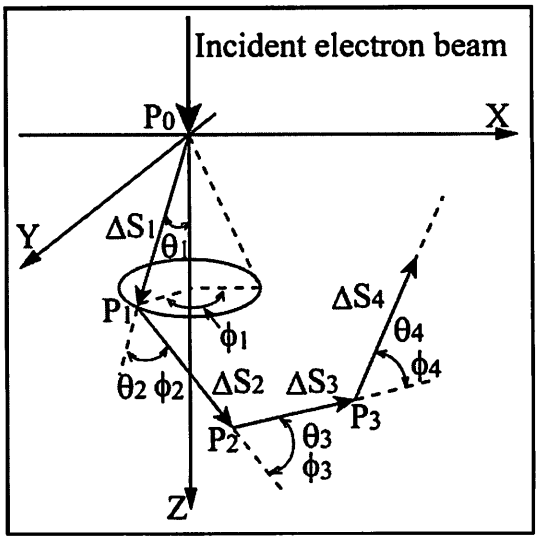

Fig. 1: The schematic of electron beam scattering

We calculate the energy loss for all scattering process. We assume the dipoles were excited in the center between scattering positions, such as P_1 and P_2 in Fig. 1. The number of excited photons G are given by[2]

$$G = \frac{\Delta E}{3E_{BG}} \quad (1)$$

where ΔE is energy loss and E_{BG} is band gap of material. The dipole polarization is random. We analyzed light scattering for each dipole by FDTD method. The light intensity distribution of fluorescence film was obtained by adding the each calculation result. We coat the gold thin film on the fluorescent film. The thickness of gold thin film is 20 nm. We chose SiN as the fluorescent film. The wavelength of the nanometric light source is 337 nm.

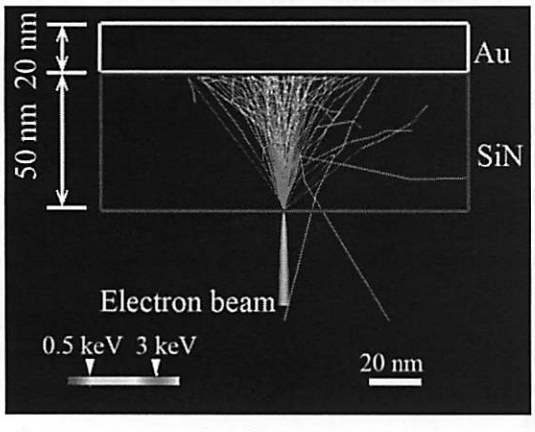

Fig. 2: The result of electron beam scattering by Monte Carlo method

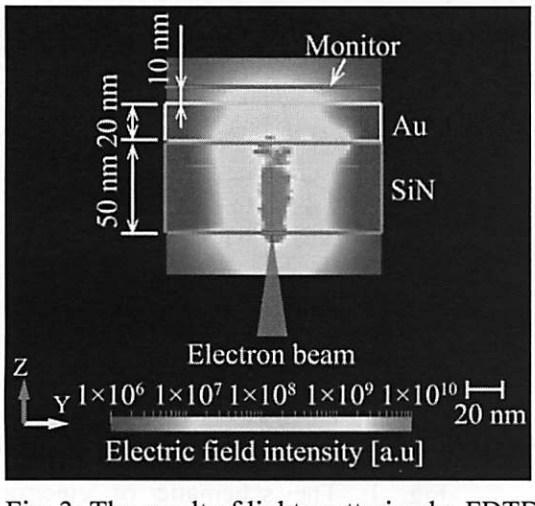

Fig. 3: The result of light scattering by FDTD method

3. Simulation result

Figure 2 shows the result of three dimensional analysis of electron beam scattering. The thickness of SiN is 50 nm, the thickness of gold thin film is 20 nm. Accelerating voltage is 3 keV. From the results shown in Fig. 1, all the electrons are stopped by the gold thin film.

Figure 3 shows the result of light scattering of dipoles that are generated by electron beam scattering. From Fig. 2, we can find that the light intensity is large at nearly gold thin film. This is because the reflected electrons by the gold thin film also excited the dipoles near the interface between SiN and gold film,.

We measured the electric field intensity at the plane which is 10 nm away from the surface of gold thin film. The full width at half maximum of excitation light spot is 47.1 nm.

4. Conclusion

The electron beam transmission is eliminated by coating the gold thin film on the fluorescent film. The thickness of gold thin film is 20 nm.

To coat the gold thin film on the fluorescence film, the full width at half maximum of excitation light spot is 47.1 nm. EXA optical microscope can realize less than 50 nm resolution.

We have developed the new analysis method combined Monte Carlo method and FDTD method. The Monte Carlo method analyzed the electron beam scattering, and FDTD method analyzed fluorescence generated by electron scattering.

Reference

[1] W.Inami, K.Nakajima, A.miyakawa, and Y.Kawata, Opt. Express 18, 12897 (2010)

[2]David C. Joy, "Monte Carlo modeling for electron microscopy and microanalysis", OXFORD (1995)

Image restoration method for high resolution image in digital holographic microscope

Do-Hyung Kim[1], Sungbin Jeon[2], Sang-Hyuk Lee[1]
Kyoung-Su Park[2], No-Cheol Park[2], Hyunseok Yang[2] and Young-Pil Park[2]
[1] Center for Information Storage Device, Yonsei University, Seoul, 120-749, Korea
[2] Department of Mechanical Engineering, Yonsei University, Seoul, 120-749, Korea
Phone: +82-2-2123-4677, Fax: +82-365-8460, E-mail: pnch@yonsei.ac.kr

Abstract

This paper introduces the image restoration method in digital holographic microscope. Suggestion of research uses the exact PSF function as image filter to compensate the image degradation by optical system of microscope. Phase shift digital holographic microscope system is constructed to apply this restoration method. From the experimental results, improvement of image resolution could be verified.

1. Introduction

From the first research of holography by Dennis Gabor [1], holography has studied in various applications. Digital holography is one technic of holography. Digital holography uses the CCD as the material to record the hologram and reconstructs the information by optical or numerical processing [2]. This method has advantage in the limitation of the recording material and reprocessing by computational method.
Digital holographic microscopy is one of the most desirable applications in digital holography. Digital holographic microscopy would provide the 3D information of the sample. It would be useful in many research areas. Resolution of digital holographic microscopy is strongly depended on size of CCD, pixel pitch, and sampling rate. In several researches, these factors are analyzed [3] In the imaging system, quality of the image is limited by spec of optical components. In other word, all optical components limit the performance of image quality which is equally applied in digital holographic microscope.

In this paper, image restoration method is proposed to avoid the limitation of optical components and achieve the high resolution.

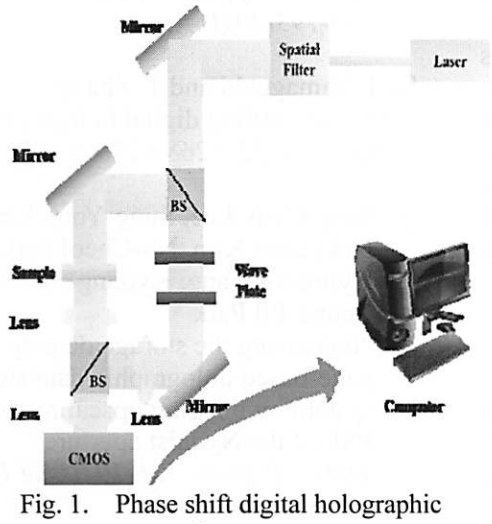

Fig. 1. Phase shift digital holographic microscpy

2. Phase shift digital holographic microscopy

The schematic view of experimental setup is shown in Fig. 1. 4-step phase shifting method is used in system. 532nm green laser is used as light source. 1536*1024 (pixel pitch 9um) resolution CCD camera is used as the sensor. Phase shifting is performed by 2 kinds of wave plates. Object lens is 20X microscope lens USAF chart is adapted as the target sample.

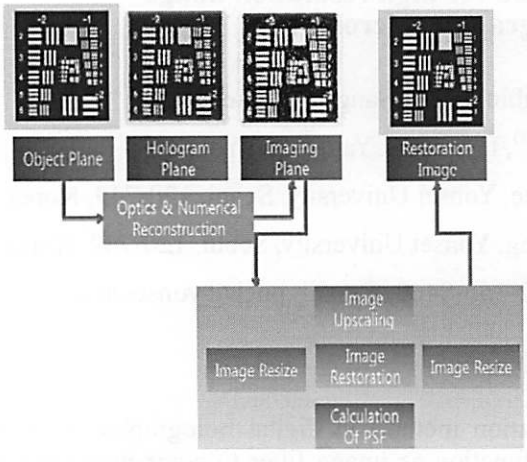

Fig. 2. Image restoration process

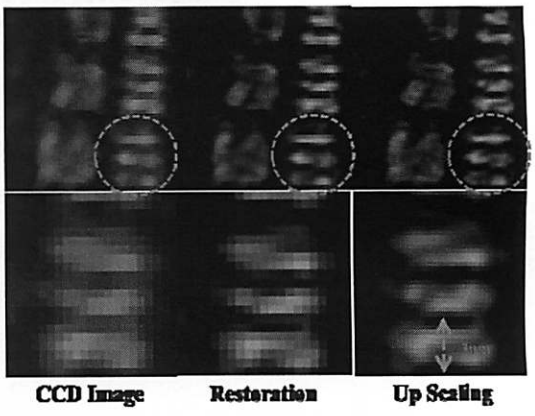

Fig. 3. Experimental results of image restoration

Hologram data is obtained by this method [4]. Obtained hologram data contain both information amplitude and phase of object. From the hologram, 3D information is reconstructed numerically by Fresnel diffraction.

3. Image Restoration process and Upscaling

Obtained hologram contains the optical property of optical system. In imaging system, image can be achieved by convolution of PSF function and original image. Obtained image is degraded by PSF function of optical system.
To avoid the degradation of image quality, this paper suggests the restoration method. Processing diagram of suggested method is shown in Fig. 2. Exact PSF function is obtained by commercial optical simulation software. Upscaling method is also adapted to improve the resolution of the reconstructed image. Fig. 3 shows the experimental results of original image and restoration image. Restoration image shows the higher resolution than original image.

4. Conclusion

In this paper, we suggest the restoration method to avoid the degradation of image quality by optical system. To compensate the degradation of the image quality, PSF function used as the image filter. Restoration image is obtained by de convolution of original image and PSF function. For improving the resolution of restored image upscaling method is used. From the experimental results, we confirm the improvement of image resolution.

Reference

[1] Gabor D "A new microscopic principle" *Nature 161: 777-778 (1949)*

[2] Ulf Schnars "Direct phase determination in hologram interferometry with use of digitally recorded holograms", *JOSA. Vol. 11, No.7 2011-2015 (1994)*

[3] Yan Hao and Anand Asundi "Resolution of a digital holography system", *Applied Optics Vol. 50, No. 2 183-193(2011)*

[4] I. Yamaguchi and T. Zhang, "Phase-shifting digital holography", *Opt. Lett. 22, 1268-1270 (1997)*

[5] Sang-Hyuk Lee, Sung-Yong Lim Nakyeong Kim, No-Cheol Park, Hyunseok Yang, Kyoung-Su Park, and Young-Pil Park "Increasing the storage density of a page-based holographic data storage system by imaging upscaling using the PSF of the Nyquist aperture" *Optics Express, Vol. 19, Issue 13, 12053-12065 (2011)*

O-14

Cathodeluminescence Imaging of Metallic Nanostructures

Ryuji Noda[1*], Syota Fukada[1], Yasunori Nawa[1], Atsushi Ono[2,3], Wataru Inami[2,3], Du Guan Xiang[4], Shin Saito[4], and Yoshimasa Kawata[1,3]

[1)]Department of Mechanical Engineering, Faculty of Engineering, Shizuoka University
[2)]Division of Global Research Leaders, Shizuoka University
[3)]CREST, Japan Science and Technology Agency
3-5-1 Johoku, Naka-ku, Hamamatsu, Shizuoka 432-8561, Japan
[4)]Department of Electronic Engineering, Graduate School of Engineering, Tohoku University
6-6-05 Aoba, Aramaki, Aoba-ku, Sendai, Miyagi 980-8579, Japan
TEL&FAX: +81-53-478-1076
*e-mail: kawata@eng.shizuoka.ac.jp

Abstract

The purpose of this research is to analyze the excitation property of a surface plasmon (SP) on a nanometer scale structure. The SP luminescent property of one-dimensional grating structure of the gold thin film was investigated. We succeeded in observation with 200 nm of spatial resolution and obtained cathodeluminescence (CL) image of gold nanorods.

1. Introduction

Recently, a waveguide and a filter with SP have been developed. Since a metallic nanostructure is used for the waveguide and the filter, it is necessary to investigate the SP excitation property in a metallic nanostructure.

SP is generally excited by light. Since the excitation area of SP is comparable as the wavelength of light, it is difficult to investigate the SP excitation property of the nanostructure below the wavelength of light.

The purpose of this research is to analyze the excitation property of a SP on a nanometer scale structure. An electron beam is used to overcome the diffraction limit of the light. This is because a spot size of the electron beam can be less than that of the light. The electron beam can be focused to a spot size in the region of a few nanometers. The focused electron beam locally excites a SP at the surface of a metallic nanostructure. Therefore, the SP excitation property in a nanostructure smaller than the wavelength of light can be analyzed.

2. The observation principle of cathodeluminescence

Figure. 1 shows the observation principle of SP. The electron beam is focused at the surface of the metallic structure, and excites a SP. When a SP restores to its former state, emits a CL. The emission spectrum depends on a nanostructure. An optical image is built by raster scanning of an electron beam. The excitation property is analyzed from this information.

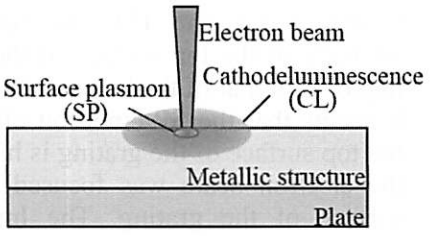

Fig. 1 The observation principle of SP. When a surface of gold is irradiated with an electron beam, SP is generated and propagates at the surface.

3. Experimental setup for the SP property on metallic nanostructure

Figure. 2 shows the schematic diagram of a experimental setup. In this experiment, the scanning electron microscope (SEM) was used for irradiation of an electron beam. An electron beam was focused on a sample surface with an object lens. The light, which was excited from a sample is collected with a lens built into the optical stage, and a

photo-multiplier (PMT) detects the light. An optical image is produced by synchronizing acquisition of the PMT signal and an electron beam scanning.

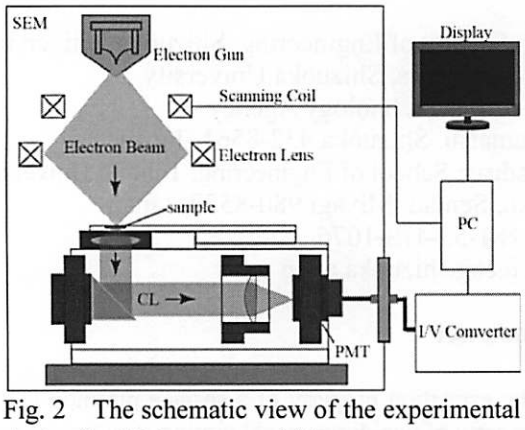

Fig. 2 The schematic view of the experimental device for CL image acquisition.

4. Experimental results of SP emission from grating structure

Figure. 3(a) shows the optical image of SP emission from one-dimensional grating, and Figure. 3(b) shows the line profile along the line indicated (a). The light emission which caused by SP scattering on rough surface of the gold film was measured. To make the grating, we dug trenches on the gold film with electron beam lithography. In figure. 3 (a) and (b), the luminescence intensity of the top surface of the grating is higher than that of the bottom of the trenches. It seems that the SP emission efficiency on the top surface of the grating is high because the electron beam was focused on the top surface of the grating. The luminescence intensity in the top surface of the grating is constant in every position. From this result, SP emission was generated of the top surface of the grating.

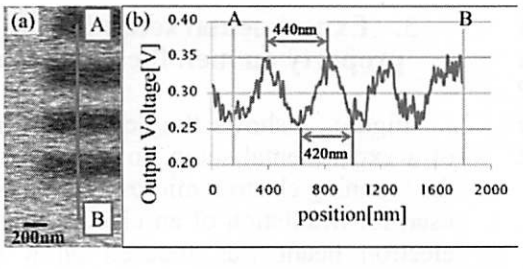

Fig. 3 (a) The CL image of the sample acquired in this experiment. (b) The line profile of the portion of the red line of Fig. 3.

5. Synthesis of gold nanorods

To reveal the SP excitation property in gold nanorods, we produced gold nanorods. Gold nanorods have advantages to control the SP band. So, these are used for bio sensing or imaging.

Gold nanorods were synthesized by seed-mediated growth method. Impurities were removed by centrifugal separation. Natural seasoning was carried out after being dropped at a silicon wafer. Figure. 4 shows the SEM image of gold nanorods.

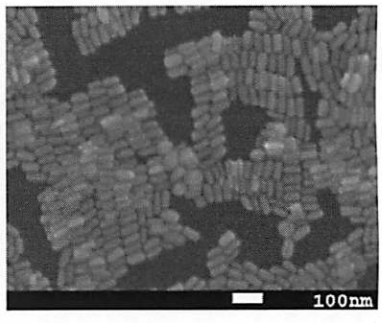

Fig. 4 The SEM image of synthesized gold nanorods. Sizes were about 60 nm at long axis, about 22 nm at short axis, and the aspect ratio is 2.7. The absorption peak was in the wavelength of 520 nm and 700 nm.

6. Conclusion

In this research, we acquired the CL image which is emitted from a gold thin film with one-dimensional grating structure. The luminescence intensity in the surface of a gold thin film was constant in every position. From this result, the light emission was caused by SP scattering rough surface of gold film.

Furthermore, we synthesized gold nanorods to investigate its SP.

From now on, the SP excitation property of gold nanorods will be measured.

Reference

[1] N. Yamamoto, OYO BUTURI. **75** (2006) 41.

[2] B. Nikoobakht, M. El-Sayed, Chem. Mater **15** (2003) 1957-1962.